ACS OMEGA

Article

Cite This: ACS Omega 2019, 4, 6084−6091

http://pubs.acs.org/journal/acsodf

High Water Resistance of Monoclinic $CsPbBr_3$ Nanocrystals Derived from Zero-Dimensional Cesium Lead Halide Perovskites

Liuli Yang,[†,∥] Ting Wang,[‡,∥] Qiuhong Min,[†] Bitao Liu,[§] Zhichao Liu,[†] Xiaotong Fan,[†] Jianbei Qiu,[†] Xuhui Xu,[†] Jie Yu,*[,†] and Xue Yu*[,†]

[†]Faculty of Materials Science and Engineering, Kunming University of Science and Technology, No. 68, Wen Chang Rd., Kunming 650093, China

[‡]Department of Applied Physics, The Hong Kong Polytechnic University, No. 11 Yu Cai Rd., Kowloon 999077, Hong Kong, China

[§]Engineering Research Center of New Energy Storage Devices and Applications, Chongqing University of Arts and Sciences, No. 319, Honghe Avenue, Chongqing 402160, China

Supporting Information

ABSTRACT: An all-inorganic cesium lead halide perovskite is particularly attractive as an alternative to next-generation display with high quantum yields and color purity for lasers, light-emitting diode (LED) devices, and single-photon sources. Unfortunately, the vulnerable properties induced by moisture limit the hopeful application of $CsPbBr_3$, especially for high-performance devices. In this work, a monoclinic $CsPbBr_3$ derived from hexagonal Cs_4PbBr_6 with the assistance of water was presented. Moisture-induced decomposition and phase segregation were recorded at the atomic level in detail. Moreover, the obtained monoclinic $CsPbBr_3$ nanocrystals (NCs) are demonstrated to be decorated with hydroxyl (OH) ligands, which provide a valid approach for the resistance to further moisture attack. The highly stable $CsPbBr_3$ NCs could preserve the photoluminescence intensity above 97% even after the sample was deposited in water for 30 days. Furthermore, a white LED constructed with the as-prepared green-emitting $CsPbBr_3$ and a commercial N628 red phosphor demonstrate the monoclinic $CsPbBr_3$ as a compelling material platform well suited to applications as next-generation light emitters.

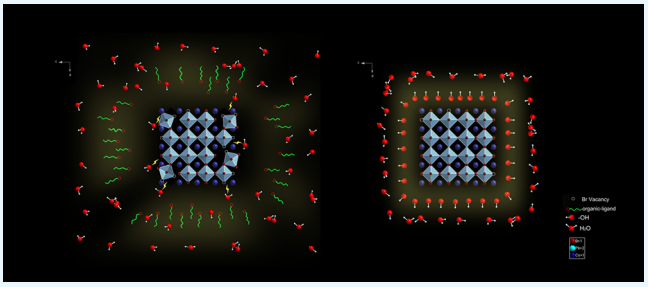

INTRODUCTION

All-inorganic perovskites combined with unique optical properties, including narrow emission bands and extremely strong emission intensity by controlling the composition and size, have gained surging research interest and also been demonstrated to be ideal materials for light-emitting devices, photodetectors, and lasers.[1−6] One, particularly, interesting class of metal halide perovskites consists of $CsPbBr_3$ nanocrystals (NCs), which have composition-tunable emission wavelength. Unfortunately, perovskite materials lack long-term stability under ambient operation conditions for the degradation induced by moisture, heat, and light.[7−9] The vulnerable properties induced by moisture are related to the structural phase stability, quantum efficiency, and surface defects, which further limit the hopeful application of $CsPbBr_3$, especially for high-performance devices.[10−13]

One of the major factors curtailing the stability of metal halide perovskites is believed to be their low formation energy. Metal halide perovskite thin films lack chemical and structural stability, and thus, they are prone to undergo rapid degradation in the presence of moisture or heat.[14] Stabilizing the perovskite against moisture is an ongoing area of research. Li and co-workers prepared $CsPbBr_3$ quantum dots with high quantum efficiency modified by hydrophobic zeolites to prevent the moisture influence.[15] Zheng group demonstrated the preparation of environmentally stable $CsPbBr_3$@TiO_2 core−shell NPs by encapsulating colloidal $CsPbBr_3$ NCs with a titanium precursor.[16] Moreover, Wu's group reported exceptional moisture stable $CsPbBr_3$ film modified by the ZnO interlayer to improve device performance.[17] Quan et al. proposed that the intercalation of phenylethylammonium (PEA) between perovskite layers would introduce quantitatively appreciable van der Waals interactions. These would drive an increased formation energy that could potentially lead to improved materials stability.[18] Moreover, an inhomogeneous interface reaction (IIR) in a liquid−liquid immiscible two-phase system was developed to fabricate the perovskite-related $CsPbX_3$ (X = Cl, Br, and I) fluorophores. Notably, the IIR process is carried out at room temperature (RT) and completed within a few minutes via ionic reaction at the interface of the "aqueous phase" and the "oil phase".[19] Recently, cubic $CsPbX_3$ NCs through the chemical transformation of presynthesized

Received: February 8, 2019
Accepted: March 14, 2019
Published: March 29, 2019

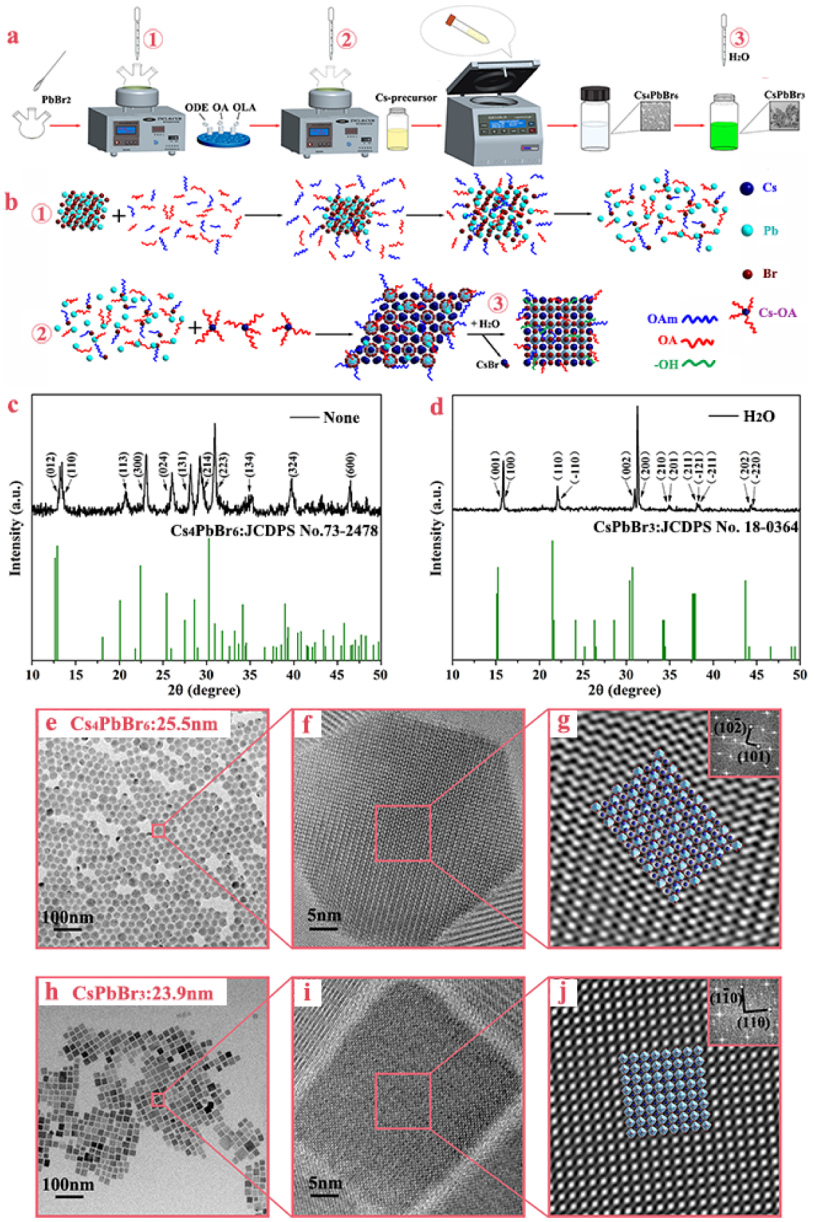

Figure 1. Schematic representation of synthesis (a) and phase transformation process (b) from Cs_4PbBr_6 to $CsPbBr_3$ NCs; XRD patterns of Cs_4PbBr_6 NCs (c), and water-induced $CsPbBr_3$ NCs (d); TEM images (e,h), HRTEM images (f,i), and iFFT images (g,j) of Cs_4PbBr_6 and $CsPbBr_3$ NCs; the insets of (g,j) are the FFT of Cs_4PbBr_6 and $CsPbBr_3$, respectively.

Cs_4PbX_6 NCs have been developed by stripping CsX through an interfacial reaction with water in a different phase.[20] As far as we know, a three-dimensional structure perovskite $CsPbX_3$ has been extensively investigated, which crystallizes in cubic, orthorhombic, and tetragonal polymorphs. However, the monoclinic phase is stable only at RT and changes into cubic phase at about 130 °C.[21] In our work, a monoclinic $CsPbBr_3$ NC transformed by injecting water into the hexagonal Cs_4PbBr_6 precursor solution synthesized via hot injection was obtained, thanks to the cleavage and recombination of the bonds of parent Cs_4PbBr_6 NCs in water. The water-driven structural evolution of a $CsPbBr_3$ single particle is observed in detail from the atomic level. The obtained monoclinic $CsPbBr_3$ NCs decorated with OH ligands exhibited excellent moisture stability compared with the counterpart derived from hot injection. Moreover, the output intensity of the green emission with negligible decline was demonstrated. Furthermore, the operational stability of perovskite light-emitting diodes (LEDs) constructed by the as-prepared green-emitting $CsPbBr_3$ and a commercial N628 red phosphor unambiguously exhibits a fascinating prospect of monoclinic $CsPbBr_3$ as next-generation light emitters.

RESULTS AND DISCUSSION

Cs_4PbBr_6 NCs are synthesized through a modified hot-injection method,[22] and then $CsPbBr_3$ NCs are obtained via a phase transformation by water induction, as shown in Figure 1a. The synthesis process of $CsPbBr_3$ NCs (Figure 1b) is divided into three stages: (1) $PbBr_2$ precursor solution is prepared in cesium oleate (Cs-OA), oleylamine (OLA), and octadecene (ODE). (2) Cs_4PbBr_6 NCs are obtained via mixing $PbBr_2$ precursor solution and Cs-OA. (3) $CsPbBr_3$ is generated by stripping CsBr from Cs_4PbBr_6 after water induction.[23] The powder X-ray diffraction (XRD) peaks of the pristine NCs of

DOI: 10.1021/acsomega.9b00370
ACS Omega 2019, 4, 6084−6091

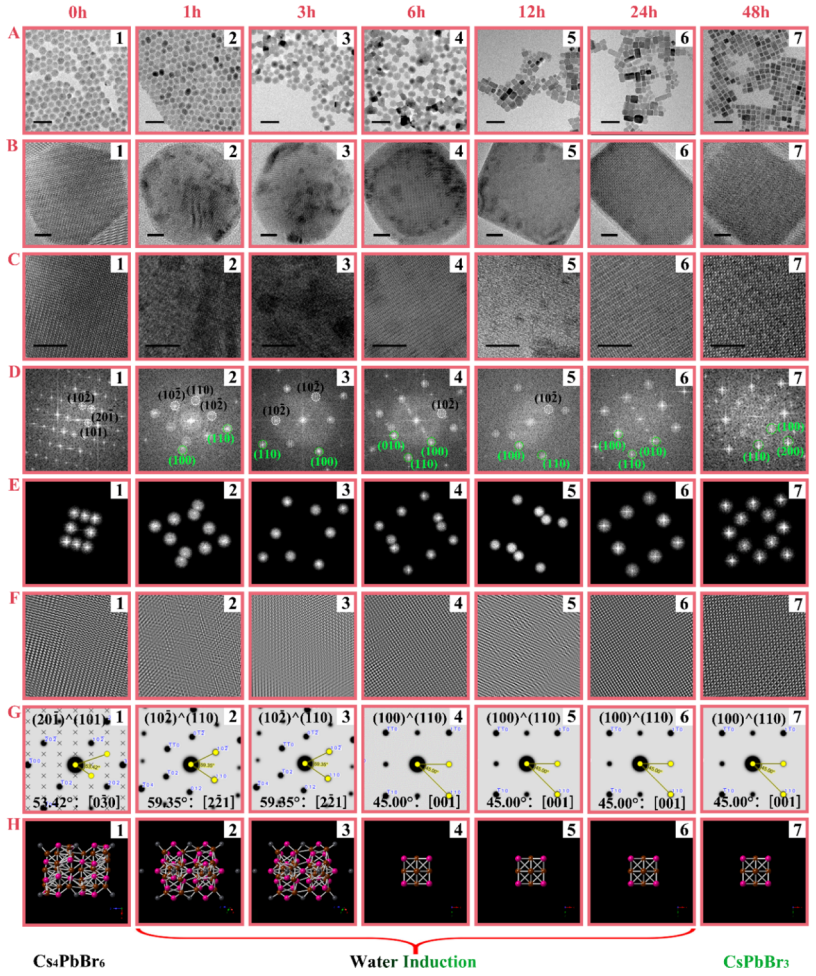

Figure 2. TEM images (A1−A7) and HRTEM images (B1−B7) of products prepared by taking aliquots out from the reaction system after water induction in 48 h, showing transformation from pure Cs_4PbBr_6 single NCs into pure $CsPbBr_3$ single NCs, respectively (A bar: 100 nm, B bar: 5 nm); local HRTEM images of products obtained from the HRTEM images (C1−C7) (bar: 5 nm); the corresponding FFT patterns of products (D1−D7); adding mask (E1−E7) [smooth edge by (pixels): 5] to get iFFT images (F1−F7) of products; the standard electron diffraction patterns (G1−G7) and the corresponding crystal structure (H1−H7) of Cs_4PbBr_6 NCs and $CsPbBr_3$ NCs.

the sample from the hot-injection method in Figure 1c match well with that of hexagonal Cs_4PbBr_6 (JCPDS no. 73-2478). After 48 h of water exposure, the XRD patterns of the final products are well consistent with the pure monoclinic $CsPbBr_3$ exhibited in the JCPDS no. 18-0364 (Figure 1d). Transmission electron microscopy (TEM) images show that the as-obtained uniform Cs_4PbBr_6 NCs have an average dimension of 25.5 nm (Figures 1e and S1a). The high-resolution TEM (HRTEM) image in Figure 1f shows a clear lattice spacing of 6.88 Å, which is in good agreement with the $(10\bar{2})$ plane of Cs_4PbBr_6. The $(10\bar{2})$ and (101) crystal planes with an angle of 90° are obviously observed, which further confirms the phase of Cs_4PbBr_6 (Figure 1g and the inset of Figure 1g). After being treated with water, the rectangular $CsPbBr_3$ NCs show the structures with an edge length of around 23.9 nm, indicating that the phase transformation was completed (Figures 1h and S1b). The measured *d*-spacing of 4.17 Å from Figure 1i can be indexed as the (110) plane of $CsPbBr_3$. The fast Fourier transform (FFT) (the inset of Figure 1j) and inverse FFT (iFFT) (Figure 1j) reflections with a *d*-spacing attributed to the $CsPbBr_3$ crystal configuration further demonstrate the completion of structure transformation. Considering the fact that CsBr NCs are soluble in water,[24] the Cs_4PbBr_6 NCs are regarded as $CsPbBr_3$ NCs rich with CsBr NCs.[21] Therefore, when the white precipitates accumulate at the bottom of the $CsPbBr_3$ NC solution during the transformation process, it is easy to assume that white precipitates are CsBr NCs (Figure S2a). Then, the result of XRD well indexed to JCPDS no. 73-0391 (Figure S2b) proved the above speculation that cubic CsBr NCs could be separated from $CsPbBr_3$ to form white precipitates. Hence, it follows that structure transformation is caused by the precipitation of CsBr NCs rather than a dissolution−recrystallization process.

The luminescence intensity of $CsPbBr_3$ NCs reaches maximum when 125 μL of deionized water was injected into 1 mL of Cs_4PbBr_6 NCs after 48 h (Figure S3). Because more CsBr NCs will be stripped from Cs_4PbBr_6 NCs when overinjected with water, quenching the green emission for the damage of the structure of Cs_4PbBr_6 NCs. Therefore, the deionized water dose for water induction is fixed to be 125 μL in our work.

To better understand the formation mechanism of $CsPbBr_3$ NCs, the structure transformation process is characterized by the monitored single particle of our sample via TEM carefully. TEM results demonstrate the morphology evolution from hexagonal Cs_4PbBr_6 NCs (before water induction) to rectangular $CsPbBr_3$ NCs (after water induction) (Figure 2A1−A7). The HRTEM study shows the structure trans-

DOI: 10.1021/acsomega.9b00370
ACS Omega 2019, 4, 6084−6091

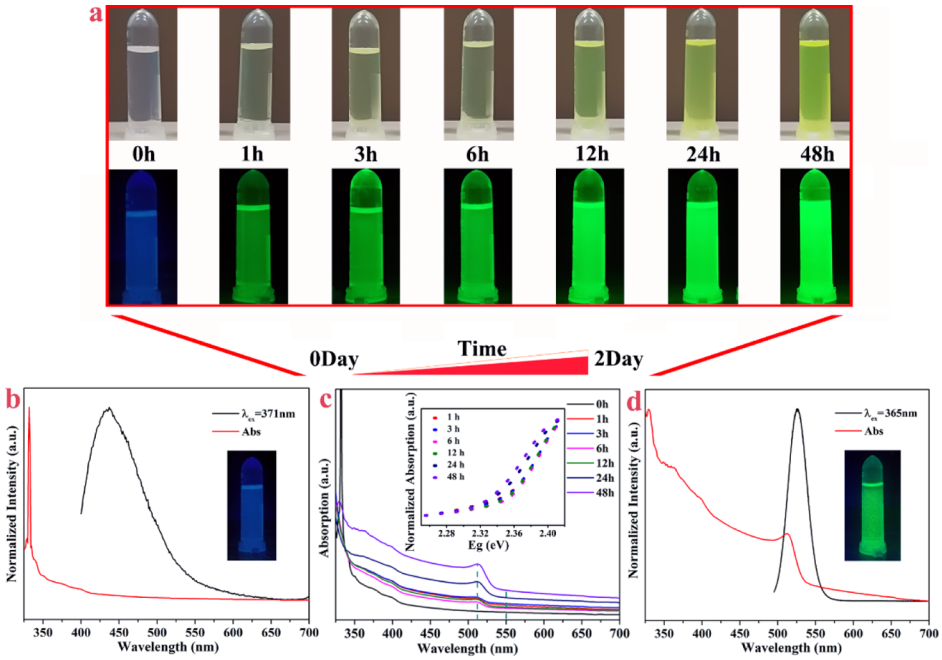

Figure 3. Photographs showing the emission color change of the sample at different times after the addition of 125 μL of water under daylight (top) and UV light (bottom) (a). Absorption (red line) and emission (black line, λ_{ex} = 371 nm) spectra of Cs_4PbBr_6 NCs in toluene (b). Absorption spectra of the sample recorded at different times after the addition of water (c). Absorption (red line) and emission (black line, λ_{ex} = 365 nm) spectra of $CsPbBr_3$ NCs in toluene (d).

formation of the Cs_4PbBr_6 single particle after water induction (Figure 2B1−B7), as there is a considerable reorganization of the lattice from Cs_4PbBr_6 to $CsPbBr_3$ NCs. Notably, the spherical particles (dark) appear attached to the surfaces of our sample (Figure 2B2−B5), which are identified as CsBr NCs[25] by the calibration of different diffraction patterns shown in Figure S4. It is consistent with the results as Cs_4PbBr_6 is CsBr-rich rather than a $PbBr_2$-deficient material.[26,27] The local HRTEM and FFT images are therefore displayed as Figure 2C1−C7,D1−D7, respectively, which discriminate kernel in the exploration. Part of the change in the crystal structure can be detected by measuring the change in interplanar distances from the diffraction pattern time series. Figure 2D1−D7 shows a time series of FFT patterns taken from the products, which are continuously exposed to 125 μL of water. The closely arranged diffraction spots show the presence of the superlattice electron diffraction patterns with double period order with diffraction boundaries parallel to the {101} planes (Figure 2D1). The superlattice electron diffraction patterns are normal to Cs_4PbBr_6 NCs[28] and show little beam-induced artifacts, which have no effect on the judgment of the phase. It is explicit that the structure of the single particle changes, even 1 h after water is introduced as shown in Figure 2D2. The first indication of change is the appearance of {100} planes belonging to the $CsPbBr_3$ phase, accompanied by the disappearance of {110} planes attributed to the Cs_4PbBr_6 phase, which indicates the gradual appearance of $CsPbBr_3$ along with the introduction of water. After 3 h of water exposure, the {102} planes of the Cs_4PbBr_6 phase in Figure 2D3 begin to become diffuse and weak, whereas the {100} planes of $CsPbBr_3$ become more prominent (Figure 2D3). The plane spacing associated with the {102} planes continuously decreases, indicating a shrinking of the Cs_4PbBr_6 lattice, possibly due to the loss of CsBr in the crystal structure. Subsequently, {102} planes of Cs_4PbBr_6 are subdued widely after 12 h and are invisible altogether after 24 h of continuous 125 μL exposure; however, the corresponding diffraction peak of Cs_4PbBr_6 NCs in XRD is still noticeable[29] (Figure S5). It is ascribed to the fact that Cs_4PbBr_6 NCs have stronger X-ray coherent scattering ability than $CsPbBr_3$ NCs.[30] The whole diffraction spots of $CsPbBr_3$ are formed 48 h later, when the extra CsBr is completely stripped as shown in Figure 2D7. Hence, the transformation process of $CsPbBr_3$ is recorded completely for the first time. The iFFT images of Figure 2F1−F7 are obtained by adding a mask (Figure 2E1−E7), which show detailed structures of the products. Moreover, the correct standard electron diffraction patterns are obtained from the FFT as displayed in Figure 2G1−G7, and the matching crystal structures are obtained in Figure 2H1−H7. These results reveal that the water molecules induce the distortion of the products and finally promote the formation of regular $CsPbBr_3$ NCs with the precipitation of CsBr. Moreover, the polarity of the solvent has a slight effect on the transformation process, such as toluene and acetone, as shown in Figure S6. The transformation is independent on the injection rate, which is confirmed by Figure S7, Video S1 (rapid), and Figure S8 (slow). The above results suggest that water triggered the phase transformation only associated with the reaction time to precipitate CsBr NCs.

After 125 μL of water is slowly injected on the top of 1 mL of Cs_4PbBr_6 NC solution and gently vibrated, the colorless solution turns light yellow gradually under daylight, whereas the blue emission Cs_4PbBr_6 NC solution exhibits green emission after water was added. When Cs_4PbBr_6 NCs are stripped of enough CsBr, the $CsPbBr_3$ NCs are completely formed. At the same time, the intensity of $CsPbBr_3$ NCs increases with time under UV light (λ_{em} = 365 nm) irradiation. The intensity of the photoluminescence (PL) peak remains maximum until the formation of $CsPbBr_3$ is completed (Figure 3a). As depicted in Figure 3b, the weak blue emission at

DOI: 10.1021/acsomega.9b00370
ACS Omega 2019, 4, 6084−6091

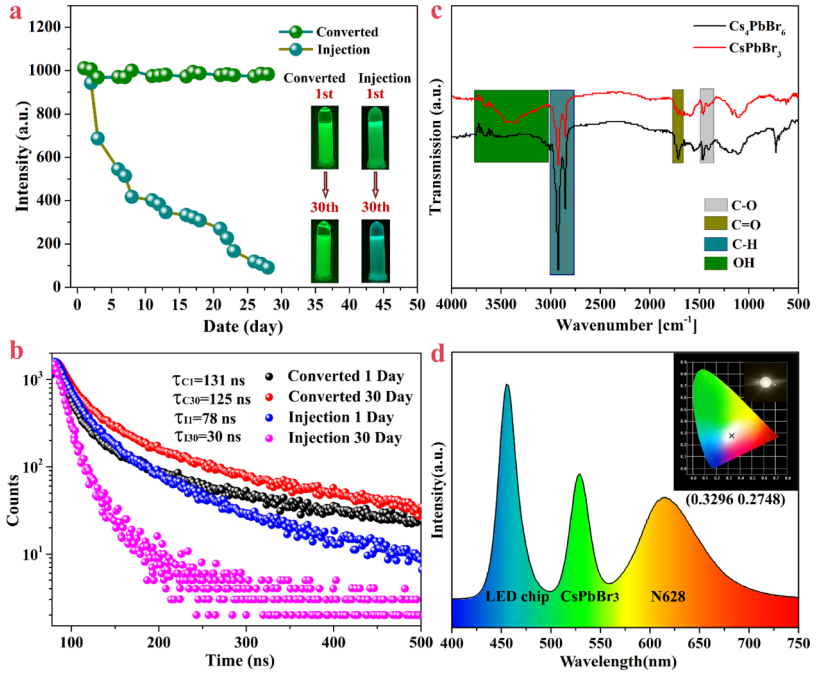

Figure 4. Time-dependent integrated PL intensity of the green emission of $CsPbBr_3$ obtained via the hot-injection and phase conversion synthesis, respectively; the insets are the photographs of the corresponding samples under UV excitation (a); PL decay dynamics of PL emission (365 nm) (b); FTIR for Cs_4PbBr_6 and $CsPbBr_3$ NCs (c); EL spectrum of the $CsPbBr_3/SiO_2$ NC-based W-LED device operated at a current level of 2.5 mA; the insets are the fabricated W-LED device and the CIE color coordinates of the prepared W-LED (d).

around 430 nm under UV light irradiation (λ_{em} = 371 nm) is recorded in Cs_4PbBr_6 and a sharp absorption peak at 331 nm is observed, which is consistent with the previous report.[20,31−33] When water is introduced into the Cs_4PbBr_6 solution, the intensity of the sharp absorption peak decreases significantly as shown in Figure 3c, which suggests that the phase transformation of Cs_4PbBr_6 NCs occurs. A small absorption peak at 525 nm emerged after water was added 1 h later, the intensity of which is enhanced along with time. At the end of the reaction after 48 h, the absorption peak at 525 nm widens and the peak at 331 nm is observed (Figure 3c). According to the Kubelka−Munk function[34] and the Tauc relation,[35] the optical band gaps are estimated (inset of Figure 3c) to be 3.68 eV for Cs_4PbBr_6 and 2.31 eV for $CsPbBr_3$ NCs (Table S1), which are well consistent with our theoretical calculated results based on density functional theory (DFT) (Figure S9). The calculated energy gaps of Cs_4PbBr_6 and $CsPbBr_3$ NCs are calculated to be 3.66 and 1.81 eV, respectively,[36−38] which are underestimated by Perdew−Burke−Ernzerhof computation. Figure 3d highlights the large shift of the band gap with the simultaneous appearance of the broad absorption and strong green PL (λ_{em} = 530 nm), which represent the formation of the $CsPbBr_3$ NCs. Moreover, the obtained $CsPbBr_3$ NCs exhibit stable green emission within 30 days in a water environment of 125 μL (Figure S10) and the PL quantum yield (~27%).

$CsPbBr_3$ NCs are dispersed in a mixed solution of 5 mL of toluene and 125 μL of water, which is then placed in an ambient environment. As shown in Figure 4a, the PL intensity of $CsPbBr_3$ NCs obtained by phase transformation from Cs_4PbBr_6 preserves 97% intensity after deposited in ambient environment for 30 days. In contrast, the emission intensity drastically decreases to 5% of the initial intensity of $CsPbBr_3$ NCs obtained through a hot-injection method under the same conditions. It implies higher stability of the phase-transformed $CsPbBr_3$ NCs. The inset of Figure 4a explicitly displays the excellent stability of the $CsPbBr_3$ NCs phase-transformed from Cs_4PbBr_6 even after 30 days. The significant reduction in PL of $CsPbBr_3$ NCs obtained through a hot-injection method is ascribed to the loss of surface ligands from the wash step[39] because of the more labile nature of the OA surface ligands. Figure 4b shows that the average lifetime of PL decay for PL emission (365 nm) remains constant within 30 days after the phase transformation, again indicating the stability of the transformed $CsPbBr_3$ NCs. To figure out the reason for the high stability of the phase-transformed $CsPbBr_3$ NCs, the Fourier transform infrared (FTIR) spectroscopy of the pristine Cs_4PbBr_6 NCs and the final produce of $CsPbBr_3$ NCs are recorded. With respect to Cs_4PbBr_6 NC samples, FTIR peaks show C−O stretching vibrations in the range of 1440−1395 cm^{-1}, C═O in 1725−1700 cm^{-1}, and C−H in 2700−3000 cm^{-1}, respectively, which is attributed to the attachment of OA of the sample. In contrast, the FTIR spectrum indicates that the intensity of the above stretching vibrations is severely weakened. Meanwhile, a broad band centered at 3400 cm^{-1} ascribed to the OH stretching vibration is found as shown in Figure 4c. According to the FTIR analysis, the inherent differences between the Cs_4PbBr_6 NCs and the transformed $CsPbBr_3$ NCs lie in the decreased OA and the increased OH group on the surface after water induction. X-ray photoelectron spectroscopy (XPS) measurements are employed to further confirm the above hypothesis (Figure S11). In Pb 4f XPS core-level spectra, two peaks of Pb $4f_{7/2}$ and $4f_{5/2}$ are observed. Both peaks of NCs can be fitted into two peaks, which demonstrate the breaking of Pb−Br bonds and formation of Pb−O bonds after water treatment.[40,41] It is apparent that majority Pb−O species are formed in the position of intrinsic Br vacancies after water treatment because the change of intensity ratio between Pb−O and Pb−Br is larger than that of Cs−Br and Pb−Br.[42] FTIR and XPS analyses showed that after water treatment, the coordination

DOI: 10.1021/acsomega.9b00370
ACS Omega 2019, 4, 6084−6091

with $CsPbBr_3$ was mainly OH rather than the organic ligand.[43−45] The schematics of ligand-free passivation of hot-injected $CsPbBr_3$ and ligand-based passivation mechanism of water-treated $CsPbBr_3$ are shown in Figure S12, respectively. It is safe to say that the OH ligand isomorphic with water is stable enough to resist further water attack as compared to OA.[46] In addition to ligand protection, water can also reduce the surface defects of perovskite NCs, resulting in high water resistance.[47] Finally, a white LED (W-LED) constructed by using the as-prepared $CsPbBr_3$ and a commercial N628 red phosphor (λ_{em} = 628 nm) with a blue-emitting GaN LED chip (λ_{em} = 460 nm) demonstrates new avenues for light-generation applications. Electroluminescence (EL) spectrum of the designed W-LED fabricated with green-emissive (emission band ranging from 500 to 560 nm) $CsPbBr_3$ NCs and commercial N628 phosphor pumped with the blue LED chip is shown in the inset of Figure 4d. Noticeably, the EL spectrum of the LED device inherits the narrow emission peaks from their EL characteristics at a driving current of 2.5 mA, achieving a full width at half-maxima of 78, 28, and 23 nm for red, green, and blue emission, respectively (Figure 4d). The Commission Internationale de L'Eclairage (CIE) chromaticity diagram of the above WLED and the CIE color coordinate are calculated to be (0.3296 0.2748) (the inset of Figure 4d). Figure S13 shows that LED assembled from transformed $CsPbBr_3$ is much more stable than that assembled from $CsPbBr_3$ synthesized via hot injection. Because of their outstanding photophysical properties, the transformed $CsPbBr_3$ NCs have been regarded as one of the potential candidates for next-generation lighting and display technology.

CONCLUSIONS

In conclusion, we directly observe the phase conversion of monoclinic $CsPbBr_3$ NCs by water-triggered chemical transformation from hexagonal Cs_4PbBr_6. The high water stability of $CsPbBr_3$ NCs is attributed to the protection of the surface OH groups, which act as ligands to participate in Pb coordination, contributing strong water resistance. The value of this work is the first detailed record of structural changes in perovskites during the continuous transformation process. The observation of the single particle conversion provides a clear proof to understand the transformed mechanisms, which offers a reference in the fabricating stable perovskites. Our findings might provide a viable source for improving the water stability and optical performance of $CsPbBr_3$ NCs, which could be employed as the next generation of lighting and displays.

EXPERIMENTAL SECTION

Chemicals. The chemicals used are as follows: lead(II) bromide ($PbBr_2$, Aladdin, 99.999%), cesium carbonate (Cs_2CO_3, Aladdin, 99.99%), ODE (Aladdin, 90%), OLA (80−90%), oleic acid (OA, Aladdin, AR), toluene (Chengdu Chemical, AR), acetone (Tianjing Chemical, AR), and room-temperature-vulcanizing (RTV) silicone rubber (Kafuter). All chemicals were used without any further purification.

Synthesis of $CsPbBr_3$ NCs. All syntheses were performed in air without any predried chemicals or solvents. In a typical synthesis, $PbBr_2$ (0.3 mmol) was dissolved in 0.5 mL of ODE, 1 mL of OA, and 1.5 mL of OLA in a 20 mL vial on a hot plate set at 100 °C. After $PbBr_2$ was completely dissolved (around 120 °C), the vial was moved to a RT hot plate, and the solution was allowed to cool. When the temperature reached the optimal value, 0.75 mL of Cs-OA (0.8 g of Cs_2CO_3 dissolved in 8 mL of OA in a 20 mL vial on a hot plate set to 190 °C) was swiftly injected. After about 5 s, the reaction turned turbid green and was quickly cooled down after 0−10 min to RT with a cold water bath. The NCs were directly washed via centrifugation (at 6000 rpm for 15 min), followed by redispersion in 5 mL of toluene (or acetone).

Synthesis and Purification of Cs_4PbBr_6 NCs. All syntheses were performed in air and without any pre-dried chemicals or solvents. In a typical synthesis, $PbBr_2$ (0.1 mmol) was dissolved in 0.5 mL ODE, 1 mL OA and 1.5 mL OLA in a 20 mL vial on a hot plate set at 100 °C. After $PbBr_2$ was completely dissolved (around 120 °C), the vial was moved to a RT hot plate, and the solution was allowed to cool. When the temperature reached the optimal value, 0.6 mL of Cs-OA (0.8 g Cs_2CO_3 dissolved in 8 mL of OA in a 20 mL vial on a hot plate set to 190 °C) was swiftly injected. After about 30 s, the reaction turned turbid white and, depending on the required size, was quickly cooled down after 0−10 min to RT with a cold water bath. The NCs were directly washed via centrifugation (at 6000 rpm for 15 min), followed by redispersion in 5 mL of toluene (or acetone).

Synthesis of Water-Induced $CsPbBr_3$ NCs. All syntheses were conducted under ambient condition. Deionized water (125 μL) was directly injected into 1 mL of Cs_4PbBr_6 solution and shaken. The final $CsPbBr_3$ solution was redispersed in 1 mL of toluene (or acetone).

Fabrication of W-LED. Dried green Cs_4PbBr_6 NCs and red N628 powders were mixed and dispersed thoroughly in a transparent RTV silicone rubber, and then the obtained mixture was coated onto the blue GaN chip. Finally, the GaN chip was cured at RT for 60 min.

Powder XRD. XRD patterns were performed using a D8 Focus diffractometer (Bruker) with Cu Kα radiation (λ = 0.15405 nm) in the 2θ range from 10° to 50°.

Optical Absorption Spectroscopy. The spectra were recorded using a HITACHI U-4100 UV−vis−NIR spectrophotometer with an integrated sphere in diffuse-reflectance mode. Samples were prepared by diluting the NC solution toluene in 1 cm path length quartz cuvettes.

Transmission Electron Microscopy. The particle morphology and size were studied with field emission TEM and HRTEM, carried out using a TECNAI G2F30 S-TWIN operating at 300 kV. The samples were prepared by drop-casting diluted NC suspensions onto 400 mesh ultrathin/holey carbon-coated copper grids for conventional TEM imaging and HRTEM imaging.

PL Measurements. The PL spectra were taken on a Hitachi F-7000 fluorescence spectrophotometer.

FTIR Spectroscopy. FTIR spectra were recorded by a Nicolet iS 10 FTIR spectrometer.

X-ray Photoelectron Spectroscopy. XPS analysis was carried out using a Thermo Fisher Scientific K-Alpha+ Al Kα X-ray source ($h\nu$ = 1486.6 eV) with a 400 μm spot size and a 30 eV pass energy.

COMPUTATIONAL METHODS

The first principles calculations were performed by the plane wave pseudopotential method implemented in the CASTEP package based on the DFT. The ion−electron interactions were modeled by ultrasoft pseudopotentials for all elements. The generalized gradient approximation was adopted to describe the exchange and correlation potentials. The kinetic

DOI: 10.1021/acsomega.9b00370
ACS Omega 2019, 4, 6084−6091

energy cutoff of 450 eV and Monkhorst−Pack *k*-point meshes with a density of (4 × 4 × 1) points in the Brillouin zone were chosen.

■ ASSOCIATED CONTENT

Supporting Information

The Supporting Information is available free of charge on the ACS Publications website at DOI: 10.1021/acsomega.9b00370.

Blue emission Cs_4PbBr_6 NC solution exhibiting green emission after addition of water (ZIP)

Size distribution of Cs_4PbBr_6 NCs and $CsPbBr_3$ NCs; pictures of CsBr, Cs_4PbBr_6, and $CsPbBr_3$; XRD of CsBr and products obtained at different reaction stages; HRTEM images; FFT images; iFFT images of single NC TEM images of Cs_4PbBr_6 NCs and $CsPbBr_3$ NCs; band structure and density of states of Cs_4PbBr_6; and PL emission spectra of $CsPbBr_3$ NCs (PDF)

■ AUTHOR INFORMATION

Corresponding Authors

*E-mail: yujiekmust@163.com (J.Y.).
*E-mail: yuyu6593@126.com (X.Y.).

ORCID

Ting Wang: 0000-0002-7549-3888
Xuhui Xu: 0000-0002-0721-7304
Xue Yu: 0000-0002-9025-2556

Author Contributions

‖L. Y. and T. W. contributed equally to this work.

Notes

The authors declare no competing financial interest.

■ ACKNOWLEDGMENTS

This work was financially supported by the National Nature Science Foundation of China (61565009 and 11664022), the Foundation of Natural Science of Yunnan Province (2016FB088), the Reserve Talents Project of Yunnan Province (2017HB011), and the Young Talents Support Program of Faculty of Materials Science and Engineering, Kunming University of Science and Technology (14078342).

■ REFERENCES

(1) Ramasamy, P.; Lim, D.-H.; Kim, B.; Lee, S.-H.; Lee, M.-S.; Lee, J.-S. All-Inorganic Cesium Lead Halide Perovskite Nanocrystals for Photodetector Applications. *Chem. Commun.* **2016**, *52*, 2067−2070.

(2) Pan, A.; He, B.; Fan, X.; Liu, Z.; Urban, J. J.; Alivisatos, A. P.; He, L.; Liu, Y. Insight into the Ligand-Mediated Synthesis of Colloidal $CsPbBr_3$ Perovskite Nanocrystals: The Role of Organic Acid, Base, and Cesium Precursors. *ACS Nano* **2016**, *10*, 7943−7954.

(3) Wei, Y.; Cheng, Z.; Lin, J. An overview on enhancing the stability of lead halide perovskite quantum dots and their applications in phosphor-converted LEDs. *Chem. Soc. Rev.* **2019**, *48*, 310−350.

(4) Li, J.; Xu, L.; Wang, T.; Song, J.; Chen, J.; Xue, J.; Dong, Y.; Bo, C.; Shan, Q.; Han, B.; Zeng, H. 50-Fold EQE Improvement up to 6.27% of Solution-Processed All-Inorganic Perovskite $CsPbBr_3$ QLEDs via Surface Ligand Density Control. *Adv. Mater.* **2017**, *29*, 1603885.

(5) Wei, Y.; Deng, X.; Xie, Z.; Cai, X.; Liang, S.; Ma, P. A.; Hou, Z.; Cheng, Z.; Lin, J. Enhancing the Stability of Perovskite Quantum Dots by Encapsulation in Crosslinked Polystyrene Beads via a Swelling-Shrinking Strategy toward Superior Water Resistance. *Adv. Funct. Mater.* **2017**, *27*, 1703535.

(6) Dursun, I.; Shen, C.; Parida, M. R.; Pan, J.; Sarmah, S. P.; Priante, D.; Alyami, N.; Liu, J.; Saidaminov, M. I.; Alias, M. S.; Abdelhady, A. L.; Ng, T. K.; Mohammed, O. F.; Ooi, B. S.; Bakr, O. M. Perovskite Nanocrystals as a Color Converter for Visible Light Communication. *ACS Photonics* **2016**, *3*, 1150−1156.

(7) Duan, J.; Hu, T.; Zhao, Y.; He, B.; Tang, Q. Carbon-Electrode-Tailored All-Inorganic Perovskite Solar Cells To Harvest Solar and Water-Vapor Energy. *Angew. Chem., Int. Ed.* **2018**, *57*, 5746−5749.

(8) Ding, J.; Du, S.; Zuo, Z.; Zhao, Y.; Cui, H.; Zhan, X. High Detectivity and Rapid Response in Perovskite $CsPbBr_3$ Single-Crystal Photodetector. *J. Phys. Chem. C* **2017**, *121*, 4917−4923.

(9) Li, B.; Zhang, Y.; Zhang, L.; Yin, L.; Yin, L. $PbCl_2$-Tuned Inorganic Cubic $CsPbBr_3$ (Cl) Perovskite Solar Cells with Enhanced Electron Lifetime, Diffusion Length and Photovoltaic Performance. *J. Power Sources* **2017**, *360*, 11−20.

(10) Zhao, J.; Cai, B.; Luo, Z.; Dong, Y.; Zhang, Y.; Xu, H.; Hong, B.; Yang, Y.; Li, L.; Zhang, W.; Gao, C. Investigation of the Hydrolysis of Perovskite Organometallic Halide $CH_3NH_3PbI_3$ in Humidity Environment. *Sci. Rep.* **2016**, *6*, 21976.

(11) Wang, S.; Bi, C.; Yuan, J.; Zhang, L.; Tian, J. Original Core−Shell Structure of Cubic $CsPbBr_3$@Amorphous $CsPbBr_x$ Perovskite Quantum Dots with a High Blue Photoluminescence Quantum Yield of over 80%. *ACS Energy Lett.* **2018**, *3*, 245−251.

(12) Li, Z.; Kong, L.; Huang, S.; Li, L. Highly Luminescent and Ultrastable $CsPbBr_3$ Perovskite Quantum Dots Incorporated into a Silica/Alumina Monolith. *Angew. Chem.* **2017**, *129*, 8246−8250.

(13) Shan, Q.; Li, J.; Song, J.; Zou, Y.; Xu, L.; Xue, J.; Dong, Y.; Huo, C.; Chen, J.; Han, B.; Zeng, H. All-inorganic quantum-dot light-emitting diodes based on perovskite emitters with low turn-on voltage and high humidity stability. *J. Mater. Chem. C* **2017**, *5*, 4565−4570.

(14) Quan, L. N.; García de Arquer, F. P.; Sabatini, R. P.; Sargent, E. H. Perovskites for Light Emission. *Adv. Mater.* **2018**, *30*, 1801996.

(15) Li, R.; Wei, Z.; Zhao, H.; Yu, H.; Fang, X.; Fang, D.; Li, J.; He, T.; Chen, R.; Wang, X. Linear and Nonlinear Optical Characteristics of All-Inorganic Perovskite $CsPbBr_3$ Quantum Dots Modified by Hydrophobic Zeolites. *Nanoscale* **2018**, *10*, 22766−22774.

(16) Li, Z.-J.; Hofman, E.; Li, J.; Davis, A. H.; Tung, C.-H.; Wu, L.-Z.; Zheng, W. Photoelectrochemically Active and Environmentally Stable $CsPbBr_3$ /TiO_2 Core/Shell Nanocrystals. *Adv. Funct. Mater.* **2018**, *28*, 1704288.

(17) Wu, Y.; Wei, Y.; Huang, Y.; Cao, F.; Yu, D.; Li, X.; Zeng, H. Capping $CsPbBr_3$ with ZnO to Improve Performance and Stability of Perovskite Memristors. *Nano Res.* **2017**, *10*, 1584−1594.

(18) Quan, L. N.; Yuan, M.; Comin, R.; Voznyy, O.; Beauregard, E. M.; Hoogland, S.; Buin, A.; Kirmani, A. R.; Zhao, K.; Amassian, A.; Kim, D. H.; Sargent, E. H. Ligand-stabilized reduced-dimensionality perovskites. *J. Am. Chem. Soc.* **2016**, *138*, 2649−2655.

(19) Chen, D.; Wan, Z.; Chen, X.; Yuan, Y.; Zhong, J. Large-scale room-temperature synthesis and optical properties of perovskite-related Cs_4 $PbBr_6$ fluorophores. *J. Mater. Chem. C* **2016**, *4*, 10646−10653.

(20) Wu, L.; Hu, H.; Xu, Y.; Jiang, S.; Chen, M.; Zhong, Q.; Yang, D.; Liu, Q.; Zhao, Y.; Sun, B.; Zhang, Q.; Yin, Y. From Nonluminescent Cs_4PbX_6 (X= Cl, Br, I) Nanocrystals to Highly Luminescent $CsPbX_3$ Nanocrystals: Water-Triggered Transformation Through a CsX-Stripping Mechanism. *Nano Lett.* **2017**, *17*, 5799−5804.

(21) Hirotsu, S.; Harada, J.; Iizumi, M.; Gesi, K. Structural phase transitions in CsPbBr3. *J. Phys. Soc. Jpn.* **1974**, *37*, 1393−1398.

(22) Akkerman, Q. A.; Park, S.; Radicchi, E.; Nunzi, F.; Mosconi, E.; De Angelis, F.; Brescia, R.; Rastogi, P.; Prato, M.; Manna, L. Nearly Monodisperse Insulator Cs_4PbX_6 (X= Cl, Br, I) Nanocrystals, Their Mixed Halide Compositions, and Their Transformation into $CsPbX_3$ Nanocrystals. *Nano Lett.* **2017**, *17*, 1924−1930.

(23) Mosconi, E.; Azpiroz, J. M.; De Angelis, F. Ab Initio Molecular Dynamics Simulations of Methylammonium Lead Iodide Perovskite Degradation by Water. *Chem. Mater.* **2015**, *27*, 4885−4892.

DOI: 10.1021/acsomega.9b00370
ACS Omega 2019, 4, 6084−6091

(24) *Alkali Metal and Ammonium Chlorides in Water and Heavy Water (Binary Systems)*; Lorimer, J. W., Ed.; IUPAC Solubility Data Series; Elsevier, 1991; Vol. *47*.
(25) Palazon, F.; Urso, C.; De Trizio, L.; Akkerman, Q.; Marras, S.; Locardi, F.; Nelli, I.; Ferretti, M.; Prato, M.; Manna, L. Postsynthesis Transformation of Insulating Cs_4PbBr_6 Nanocrystals into Bright Perovskite $CsPbBr_3$ Through Physical and Chemical Extraction of CsBr. *ACS Energy Lett.* **2017**, *2*, 2445−2448.
(26) Yang, Z.; Xu, Q.; Wang, X.; Lu, J.; Wang, H.; Li, F.; Zhang, L.; Hu, G.; Pan, C. Large and Ultrastable All-Inorganic $CsPbBr_3$ Monocrystalline Films: Low-Temperature Growth and Application for High-Performance Photodetectors. *Adv. Mater.* **2018**, *30*, 1802110.
(27) Duan, J.; Zhao, Y.; He, B.; Tang, Q. High-Purity Inorganic Perovskite Films for Solar Cells with 9.72% Efficiency. *Angew. Chem., Int. Ed.* **2018**, *57*, 3787−3791.
(28) De Graef, M.; McHenry, M. E. *Structure of Materials, An Introduction to Crystallography, Diffraction and Symmetry*; Cambridge University Press, 2012.
(29) Akkerman, Q. A.; Abdelhady, A. L.; Manna, L. Zero-Dimensional Cesium Lead Halides: History, Properties, and Challenges. *J. Phys. Chem. Lett.* **2018**, *9*, 2326−2337.
(30) Frost, J. M.; Butler, K. T.; Brivio, F.; Hendon, C. H.; Van Schilfgaarde, M.; Walsh, A. Atomistic Origins of High-Performance in Hybrid Halide Perovskite Solar Cells. *Nano Lett.* **2014**, *14*, 2584−2590.
(31) Quan, L. N.; Quintero-Bermudez, R.; Voznyy, O.; Walters, G.; Jain, A.; Fan, J. Z.; Zheng, X.; Yang, Z.; Sargent, E. H. Highly emissive green perovskite nanocrystals in a solid state crystalline matrix. *Adv. Mater.* **2017**, *29*, 1605945.
(32) Nikl, M.; Mihokova, E.; Nitsch, K.; Somma, F.; Giampaolo, C.; Pazzi, G. P.; Fabeni, P.; Zazubovich, S. Photoluminescence of Cs4PbBr6 crystals and thin films. *Chem. Phys. Lett.* **1999**, *306*, 280−284.
(33) Yin, J.; Zhang, Y.; Bruno, A.; Soci, C.; Bakr, O. M.; Brédas, J.-L.; Mohammed, O. F. Intrinsic Lead Ion Emissions in Zero-Dimensional Cs4PbBr6 Nanocrystals. *ACS Energy Lett.* **2017**, *2*, 2805−2811.
(34) Kortüm, G.; Braun, W.; Herzog, G. Principles and Techniques of Diffuse-Reflectance Spectroscopy. *Angew. Chem., Int. Ed.* **1963**, *2*, 333−341.
(35) Pankove, J. I. *Optical Processes in Semiconductors*; Courier Corporation, 1975.
(36) Murtaza, G.; Ahmad, I. First Principle Study of the Structural and Optoelectronic Properties of Cubic Perovskites $CsPbM_3$ (M= Cl, Br, I). *Phys. B* **2011**, *406*, 3222−3229.
(37) Qian, J.; Xu, B.; Tian, W. A Comprehensive Theoretical Study of Halide Perovskites ABX_3. *Org. Electron.* **2016**, *37*, 61−73.
(38) Koolyk, M.; Amgar, D.; Aharon, S.; Etgar, L. Kinetics of Cesium Lead Halide Perovskite Nanoparticle Growth; Focusing and De-focusing of Size Distribution. *Nanoscale* **2016**, *8*, 6403−6409.
(39) De Roo, J.; Ibáñez, M.; Geiregat, P.; Nedelcu, G.; Walravens, W.; Maes, J.; Martins, J. C.; Van Driessche, I.; Kovalenko, M. V.; Hens, Z. Highly Dynamic Ligand Binding and Light Absorption Coefficient of Cesium Lead Bromide Perovskite Nanocrystals. *ACS Nano* **2016**, *10*, 2071−2081.
(40) Li, M.; Zhang, X.; Matras-Postolek, K.; Chen, H.; Yang, P. Anion drived Sn^{2+} exchange reaction in $CsPbBr_3$ nanocrystals towards tunable and high photoluminescence. *J. Mater. Chem. C* **2018**, *6*, 5506−5513.
(41) Loiudice, A.; Saris, S.; Oveisi, E.; Alexander, D. T. L.; Buonsanti, R. $CsPbBr_3$ QD/AlOx Inorganic Nanocomposites with Exceptional Stability in Water, Light, and Heat. *Angew. Chem., Int. Ed.* **2017**, *56*, 10696−10701.
(42) Wu, Y.; Wei, C.; Li, X.; Li, Y.; Qiu, S.; Shen, W.; Cai, B.; Sun, Z.; Yang, D.; Deng, Z.; Zeng, H. In Situ Passivation of $PbBr_6^{4-}$ Octahedra toward Blue Luminescent $CsPbBr_3$ Nanoplatelets with Near 100% Absolute Quantum Yield. *ACS Energy Lett.* **2018**, *3*, 2030−2037.
(43) Zhai, W.; Lin, J.; Li, Q.; Zheng, K.; Huang, Y.; Yao, Y.; He, X.; Li, L.; Yu, C.; Liu, C.; Fang, Y.; Liu, Z.; Tang, C. Solvothermal Synthesis of Ultrathin Cesium Lead Halide Perovskite Nanoplatelets with Tunable Lateral Sizes and Their Reversible Transformation into Cs_4PbBr_6 Nanocrystals. *Chem. Mater.* **2018**, *30*, 3714−3721.
(44) Mosconi, E.; Azpiroz, J. M.; De Angelis, F. Ab Initio Molecular Dynamics Simulations of Methylammonium Lead Iodide Perovskite Degradation by Water. *Chem. Mater.* **2015**, *27*, 4885−4892.
(45) Wei, Y.; Deng, X.; Xie, Z.; Cai, X.; Liang, S.; Ma, P. A.; Hou, Z.; Cheng, Z.; Lin, J. Enhancing the Stability of Perovskite Quantum Dots by Encapsulation in Crosslinked Polystyrene Beads via a Swelling-Shrinking Strategy toward Superior Water Resistance. *Adv. Funct. Mater.* **2017**, *27*, 1703535.
(46) Eperon, G. E.; Habisreutinger, S. N.; Leijtens, T.; Bruijnaers, B. J.; van Franeker, J. J.; deQuilettes, D. W.; Pathak, S.; Sutton, R. J.; Grancini, G.; Ginger, D. S.; Janssen, R. A. J.; Petrozza, A.; Snaith, H. J. The Importance of Moisture in Hybrid Lead Halide Perovskite Thin Film Fabrication. *ACS Nano* **2015**, *9*, 9380−9393.
(47) Liu, Y.; Li, F.; Liu, Q.; Xia, Z. Synergetic Effect of Postsynthetic Water Treatment on the Enhanced Photoluminescence and Stability of $CsPbX_3$ (X= Cl, Br, I) Perovskite Nanocrystals. *Chem. Mater.* **2018**, *30*, 6922−6929.

DOI: 10.1021/acsomega.9b00370
ACS Omega 2019, 4, 6084−6091